A viscous froth model for dry foams in the Surface Evolver

Cox, Simon

DOI:
10.1016/j.colsurfa.2004.12.061

Publication date:
2005

Citation for published version (APA):
Cox, S. (2005). *A viscous froth model for dry foams in the Surface Evolver*. 81-89.
https://doi.org/10.1016/j.colsurfa.2004.12.061

A Viscous Froth Model for Dry Foams in the Surface Evolver

S.J. Cox

Department of Physics, Trinity College, Dublin 2, Ireland.

Abstract

An implementation of the recent viscous froth model of Kern et al. [1] in the Surface Evolver is described, along with examples of the simulations that can be achieved. In particular, results are given for steady shear of both periodic and confined staircase structures, and contrasted with the quasi-static case. Also discussed are the case of Couette shear and the relaxation due to coarsening after an initial step-strain. It is shown how the viscous froth model allows the investigation of strain-rate dependent effects and that it gives improved resolution of the topological events which govern the foam's evolution, leading to structures that could not previously have been predicted.

Key words: Foam, Viscosity, Rheology, Surface Evolver

1 Introduction

The flow of foams is seen in many processes, and its use in major industries means that an understanding of foam rheology is of paramount importance. Although foams are disordered materials, they have well-defined equilibrium laws which allow their static structure to be well-defined [2]. It is perhaps the combination of industrial importance with an attractive and precise local structure that makes foams one of the best candidates to improve our understanding of the rheology of (non-Newtonian) complex fluids.

As is well-known, foams are elastic solids at low strain. They deform plastically as the strain increases until they act as liquids at high stress, above a so-called yield stress. To model such a system we must proceed through a process of controlled approximation.

We therefore consider a dry two-dimensional (2D) foam, such as can be made by trapping bubbles between two parallel and closely spaced horizontal glass plates. The condition that the foam is dry, or of low liquid fraction, means that the junction, or Plateau border, where three films meet is of negligible size. As described in [1], we improve upon the usual *quasi-static* model of flow by considering the drag of the liquid surfaces along these glass plates to be the dominant contribution to the viscous effects present. The implementation of this *viscous froth model* in the Surface Evolver [3] will be described in detail here, along with results from simulations representing a number of experiments of interest. The advantage of using the Surface Evolver is that, even though we do *not* intend to minimize line-length subject to fixed bubble volumes, as in the more usual model of

a 2D foam, the necessary command language exists for describing and maintaining a discretized network of films, with the possibility to constrain the foam by walls and allow gas diffusion in a straightforward way.

The energy of a static 2D foam is the total length of the films. These films always meet three-fold at angles of 120° in equilibrium. In the quasi-static model of foam rheology, a small increment in strain is followed by relaxation to a local minimum of film length. During each step, many neighbour-switching T1 transformations may occur, but their precise *order* of occurrence is not resolved. Viscous froth models attempt to improve upon this description through the addition of viscous drag on the structure, as well as the more obvious possibility to model strain-rate dependent effects.

Previous attempts to model the viscous rheology of 2D foams include the notable examples of Kawasaki and co-workers [4, 5] and Cantat and Delannay [6], who implemented the *vertex model* first described by Fullman [7]. In this case the films are straight lines connected three-fold at vertices (Plateau borders) at which the viscous drag acts. In the limit of high liquid fraction (wet foams), the *bubble model* of Durian [8] sheds light on the rheology close to the rigidity loss transition [9] by considering the bubbles as circular discs with spring-like contacts. An alternative approach is the use of the Potts model [10] or Lattice Gas model [11], but the viscous dissipation is not controllable in these systems.

In the model of Kern et al. [1], the drag is considered to act on the whole length of the film, as justified by the experiments of Cantat et al. [12]. Moreover, the approximation is made that since the vertices are of negligible size, the drag on them is also negligible and the films therefore meet at 120° as in the quasi-static case. It is this condition, along with the roughly equivalent statement that films meet solid walls at 90°, that appears to be most contentious. Without reiterating the justification [1], we state here that before incorporating further physics to describe the motion of the vertices, as described briefly below, it is instructive to consider the viscous froth model as described here, even if only as a "toy model". As we describe in this paper, the simulations based upon this simple model lead to interesting conclusions that will provide a base upon which further details of the microscopic processes occurring can be built.

These microscopic processes concern the motion of the surfactant within a film when it is stretched or compressed. This movement will lead to changes in the surface tension of each film [13], so that where they meet at a vertex the force balance will in general not lead to equal angles of 120°. Incorporation of such an effect also requires an analysis of the time-scale of surfactant motion in comparison to the time-scales associated with viscous relaxation (and perhaps those associated with coarsening and strain-rate): it may be that in a 2D foam experiment there is a flow of surfactant from the fluid reservoir underlying the foam, an effect which is not present in fully three-dimensional foams.

2 The viscous froth model

We consider a collection of bubbles of area A_i. They are separated by thin films of surface tension γ. Each point of each film has curvature K and there is a pressure difference across it of Δp (i.e. the difference between the pressures of the neighbouring bubbles). In equilibrium the two forces

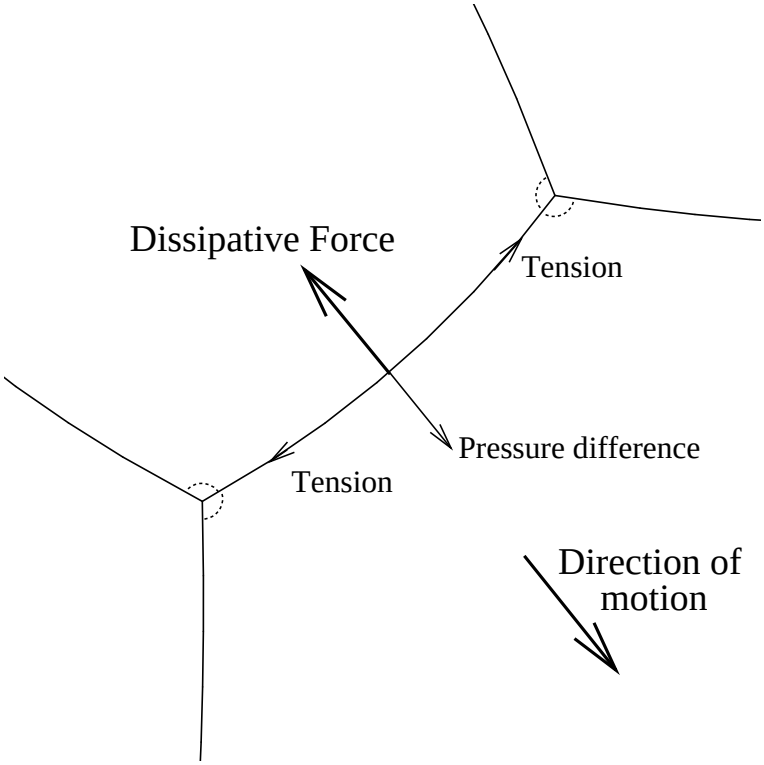

Fig. 1. The viscous froth model (2) includes a dissipative force (λv), opposing the motion. The other two terms in the force balance, applied at each point of the discretized network of films, are the surface tension γ and the pressure difference Δp, as in the Laplace law (1). We assume that the vertex angles, as indicated, remain at $120°$, but the film is not, in general, a circular arc.

represented here must balance to give the familiar Laplace Law:

$$\Delta P = \gamma K \tag{1}$$

leading to films that are arcs of circles, since the pressure difference sets the film curvature.

However, in the viscous froth model [1] the film is allowed to move with normal velocity v, experiencing a drag represented by a parameter λ. The value of λ is still somewhat open to debate, and probably depends upon parameters such as the liquid fraction and bulk viscosity as well as the precise geometry of the experiment itself [14].

A force balance in the direction of the normal for each segment of film, shown in figure 1, then leads to the following simple evolution equation:

$$\Delta P - \gamma K = \lambda v^{\alpha} \tag{2}$$

Note that we neglect and drag associated with tangential motion in the films since this introduces no change in line-length but creates complicated dynamics at the vertices.

The exponent α in the equation derives from the analysis of Bretherton [15] for the motion of bubbles in a tube. The complicated fluid dynamics that occurs when the meniscus between bubbles is perturbed by the moving bubbles permits a similarity solution relating the pressure drop along the tube to the velocity of the bubbles with an exponent of $\alpha = 2/3$. In the following, we consider the case of $\alpha = 1$ since it greatly simplifies and accelerates the numerical procedure; moreover,

Cantat et al. [12] have shown that for a typical experiment the difference between taking values of $\alpha = 1$ and $\alpha = 2/3$ is small. In future work we shall relax this restriction.

Note that the viscous froth model includes the limiting cases of (i) the ideal (quasi-static) soap froth at low velocities v and (ii) curvature-driven grain-growth when the pressure differences are negligible.

2.1 Previous work – T1s & rupture

Kern et al. [1] first applied the viscous froth model to isolated rupture (coalescence) events and T1 "neighbour swapping" topological changes. They showed that the initial dynamics after a T1 is a square-root increase in the length of the new film, followed by an exponential relaxation of the whole foam structure to equilibrium. A similar exponential relaxation is found after a coalescence event.

The most striking success, thus far, of the viscous froth model is its application to the "T1 generator" experiment in which a staircase structure of bubbles is pushed through a narrow channel containing a 180° bend [16, 1]. At low bubble velocities, experiments show that the structure passes around the bend without change of topology, as predicted by quasi-static simulations. However, at higher velocities there is a T1 close to the apex of the bend. Simulations using the viscous froth model qualitatively reproduce this behaviour, showing, for example, that the critical velocity at which a T1 occurs increases with decreasing bubble area. Quantitative agreement is now being achieved [17, 18] by comparing the length of the films as they traverse the 180° bend, to give a prediction for the drag coefficient λ (for a foam between glass plates).

2.2 Time-scales

Based upon the parameters in the viscous froth model, we extract three time-scales relevant to the experiments on foams that we will simulate (see [1] for further details). The most important is that due to the viscous relaxation of the foam structure,

$$T_\lambda = \frac{\lambda R^2}{\gamma} \tag{3}$$

where R is a length-scale associated with the bubbles; we shall choose $R^2 = \langle A \rangle$, the average bubble area.

If the foam is allowed to coarsen, a further time-scale is introduced by the diffusion constant κ. We then have

$$T_\kappa = \frac{R^2}{\gamma \kappa} \tag{4}$$

to characterize the coarsening dynamics.

Finally, if the foam is sheared, with a strain-rate $\dot{\zeta}$, the associated time-scale is given by

$$T_\zeta = \frac{1}{\dot{\zeta}}. \tag{5}$$

We next describe various applications of the model to experiments of interest, providing information about a range of simulations that are possible, and that will be explored in more detail in future work. They allow us to explore the competition between the time-scales given above.

3 Simulation results

The implementation of the viscous froth model in the Surface Evolver is described in the Appendix. It is aimed at the reader with a basic familiarity with the software. Features of the Evolver allow us to find the soap film curvatures, while each bubble's pressure is calculated by integrating the equation of motion (2) around its perimeter [1]. We introduce a length l_{min} to represents the length of a film at which a T1 process may occur and four bubbles each exchange a neighbour [19]. Increasing the parameter l_{min} could represent an increase in liquid fraction, since a T1 is initiated when the swollen Plateau borders of a wet foam touch. In our numerical simulations we will choose $\lambda = 1$ and $\gamma = 1$, without loss of generality.

We first neglect coarsening, and investigate the interaction between the time-scales associated with relaxation T_λ and strain-rate T_ζ. We then introduce coarsening and neglect strain-rate effects. We do this through simulations encompassing both periodic and solid boundaries, both mono- and polydisperse foams, and both random and ordered foam structures.

3.1 Periodic foams under simple shear

We commence with perhaps the simplest case (no coarsening, no solid boundaries): the shear of a periodic sample of foam. We prepare a doubly-periodic foam with bubbles of area $A = 0.01$. To prevent complete (hexagonal) ordering of the foam and to assist in visualizing the flow, we increase the volume of two bubbles by a factor of 1.5. The sample has unit height and width, and we shear the foam by increasing the strain parameter ζ_{xy}, as shown in figure 2(a). Strain-rates of $\dot{\zeta} = 0.5$ and $\dot{\zeta} = 5.0$ are used, giving $T_\lambda = 0.01$ and $T_\zeta = 2$ and 0.2 respectively. These simulations are also compared with the quasi-static case, in which the elastic relaxation at each step in strain is instantaneous ($T_\lambda \ll T_\zeta$).

The evolution of the foam structure in each case is shown in figure 2. It is best characterized by the change in the total energy or line-length of the structure as a function of strain, shown in figure 3. The latter shows that for a value of $T_\zeta = 2$, i.e. much greater than the relaxation time $T_\lambda = 0.01$, there is little difference in the energy of the structure, although the T1s are now well-resolved, in comparison to the quasi-static case. However, as the strain-rate increases and T_ζ decreases towards T_λ the evolution is markedly different. It is clear from the simulations that the effect of the shear does not propagate into the bulk of the foam, but instead the bubbles on the edge of the periodic cell deform rapidly, undergoing many T1 changes.

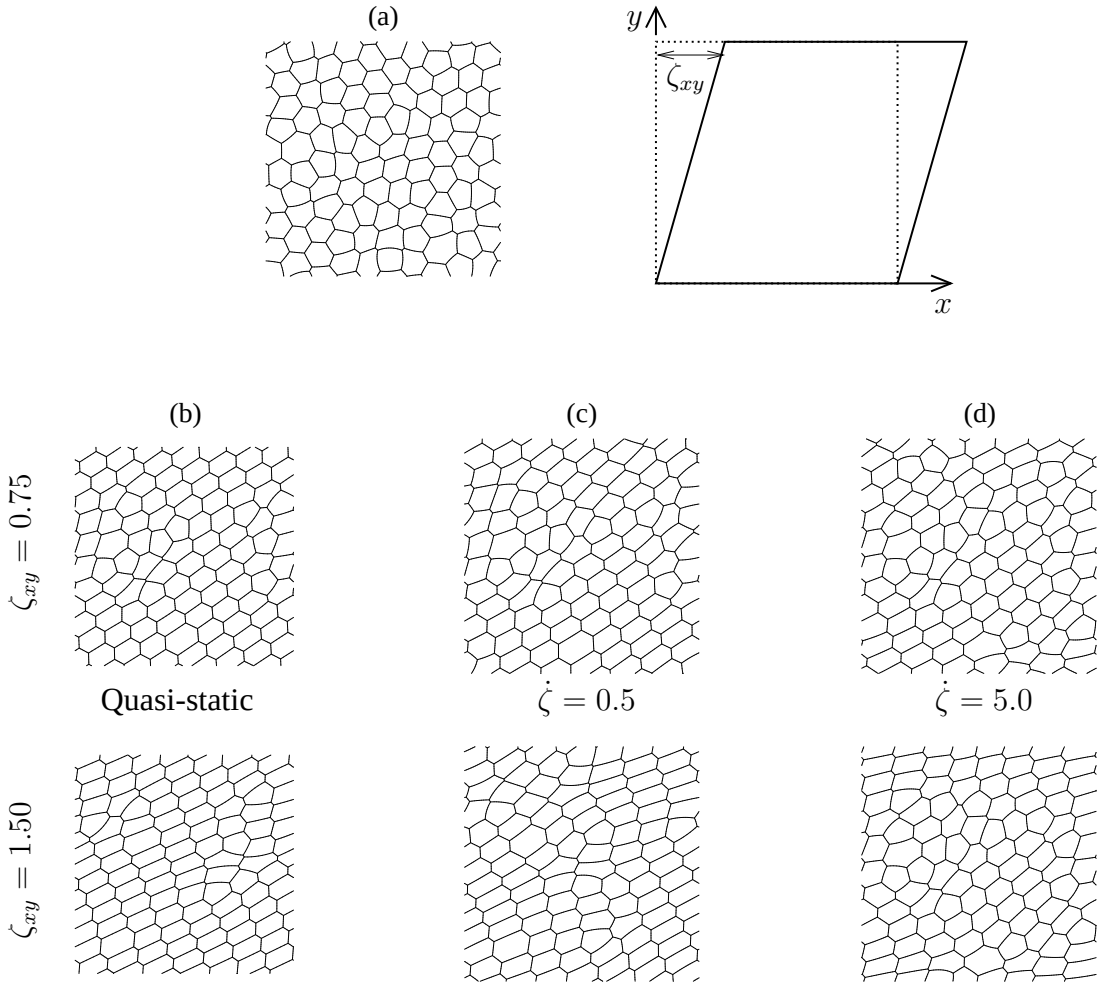

Fig. 2. (a) This periodic cluster of 100 bubbles is sheared both quasi-statically (b) and in the viscous froth (c) with strain-rate $\dot{\zeta} = 0.5$ and (d) with $\dot{\zeta} = 5.0$. Images are shown at values of strain $\zeta_{xy} = 0.75$ (upper pictures) and $\zeta_{xy} = 1.5$ (lower pictures). Note the presence of two slightly larger bubbles which show how the foam moves over time. In these snapshots from the simulations (in which the right-hand part of each image is "cut-and-pasted" on the left so that the foam sample still looks square) it is clear that the structures become different, despite starting from precisely the same configuration. Both alternate between configurations that are mostly hexagonal and those that consist of more random packings.

3.2 Annular foams under Couette shear

Motivated by recent experiments [20, 21], we study the effect of Couette shear upon a 2D foam confined within an annulus. Our intention is to investigate the distance to which T1s propagate into the bulk of the foam from the boundaries [22]. Within the same geometry, we can vary both the strain-rate, as above, and the area dispersity for an experiment in which the outer boundary of the Couette cell is rotated, described in figure 4(a).

In the Couette geometry, the stress in the foam decreases quadratically from the inner boundary, so that a simulation in a rectangular geometry is inappropriate. Even though it is the outer boundary that is moved, a quasi-static simulation shows that the foam yields close to the fixed inner boundary [23]. As the area dispersity increases, the width of the region where T1s occur persistently (the shear band) increases. With the viscous froth model, we find that there is a change in behaviour as the strain-rate is increased – if the outer boundary is moved rapidly enough, there is a

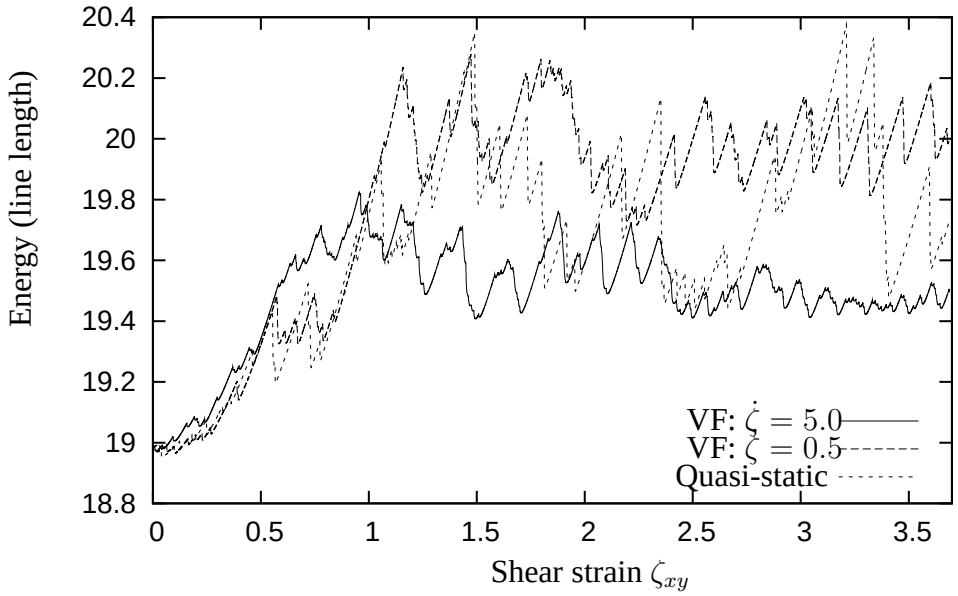

Fig. 3. The evolution of the total energy (line-length) in a periodic foam of 100 bubbles with average area 0.01, shown in figure 2, as a function of the strain-rate ζ_{xy}. The comparison is between the viscous froth equation with strain-rate $\dot{\zeta} = 0.5$, $\dot{\zeta} = 5.0$, and the quasi-static case. At low strain-rate the differences in energy are small, although significant in that the order in which T1s occur is well-defined in the viscous froth. At high strain-rate, the energy reaches a lower plateau; the simulation indicates that only the upper and lower rows of bubbles move in this case.

corresponding motion of the outer layers of bubbles and the inside of the foam remains stationary. Here we demonstrate the two extreme behaviours by comparing a viscous froth calculation at finite shear-rate with a quasi-static one. In future work we will identify the cross-over point, in terms of a critical shear-rate that depends upon area-dispersity.

Instead of simulating the whole annular foam, we consider one 15^{th} of the foam, and replicate it periodically. We take a well-annealed foam sample (i.e. in a fairly deep local energy minimum) of 144 bubbles between circles of radius 40 and 47. We define the area of each bubble by:

$$A_i = \langle A \rangle \left(1 + 2V_p(p - \frac{1}{2})\right) \tag{6}$$

for random numbers p defined uniformly in the interval $[0 : 1]$. All volumes are then scaled by a small amount to fill the shear cell. Therefore the average bubble area $\langle A \rangle$ is close to one, and the area dispersity is characterized by the parameter V_p.

After creating and annealing a sample with area-dispersity $V_p = 0.5$ and iterating to equilibirum, we fix those vertices that touch the inner and outer boundaries. Motion proceeds by moving the outer circle, and those vertices fixed to it, in a clockwise direction with strain-rate $\dot{\zeta} = 0.004$, while the inner circle and its associated vertices remain fixed, as illustrated in figure 4. We also show the results of a quasi-static calculation on a similar foam. We measure the total energy of the foam and find the radial position of each T1 as a function of the distance moved by the outer boundary, shown in figure 5. As the strain-rate increases, the T1s move from a shear-band close to the inner wall, to one close to the outer, moving, wall. There is an associated decrease in the variations in energy, after the yield stress is reached.

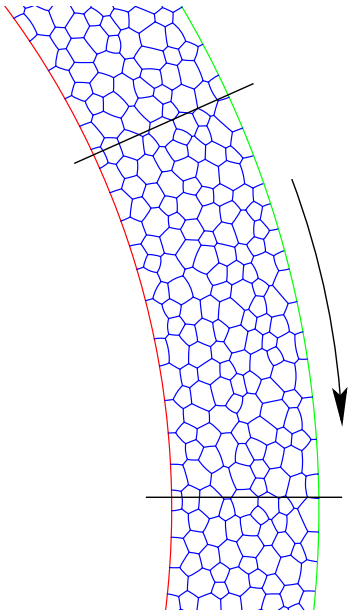

Fig. 4. The initial configuration of foam with dispersity $V_p = 0.5$ before Couette shear in which the outer boundary is moved clockwise. The solid lines show the extent of the cell used for computation, which is then replicated periodically around the annulus.

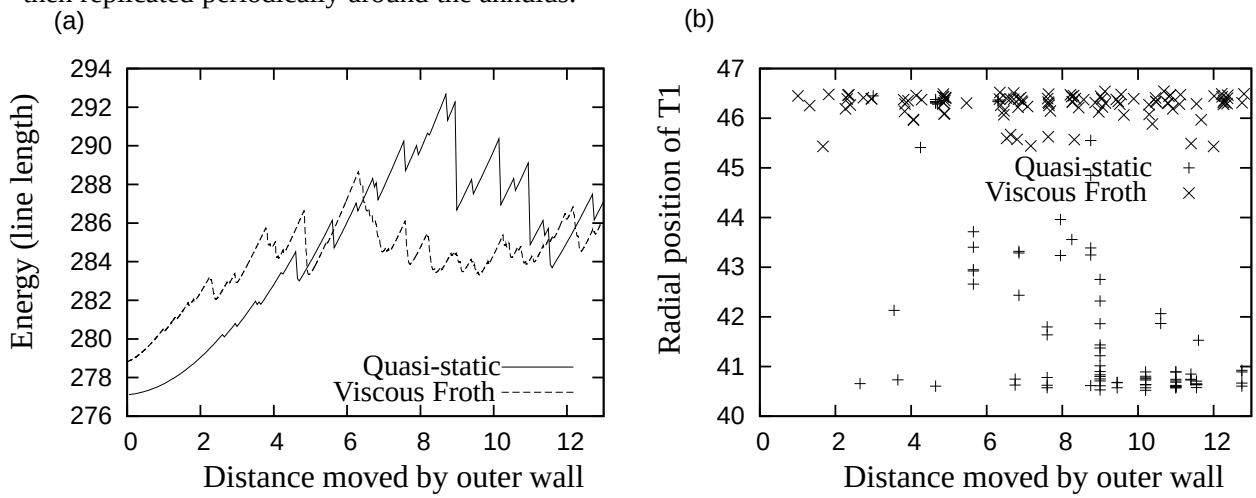

Fig. 5. (a) The energy of a foam of 144 bubbles in a Couette cell. In the quasi-static case there is a wider variation of energy, as avalanches of T1s reduce the energy rapidly. (b) The radial position of each T1 in the same simulations – the positions at which they occur are correlated with the drops in energy. For the finite shear-rate of $\dot{\zeta} = 0.0004$ in the viscous froth case, the outer wall moves fast enough that all the T1s occur close to it, rather than close to the inner, stationary, wall, after an initial transient as in the quasi-static case.

3.3 Confined staircase structures under simple shear

We consider now a regular structure confined within a channel. The staircase structure shown in figure 6 is directly related to the honeycomb structure. It is sheared by fixing the outer vertices to the bounding walls and then moving one wall and its attached vertices with strain-rate $\dot{\zeta}$. We choose four values of strain-rate and compare also with the quasi-static case ($\dot{\zeta} \to 0$). We consider the "start-up" flow, where the structure is deformed from its equilibrium state, and run the simulation until just after the second set of T1s occur.

The variation of the line-length with strain ζ, corresponding to the displacement of the moving wall divided by the wall-separation $w = 2$, is shown in figure 7(a). As the strain-rate $\dot{\zeta}$ is increased, the

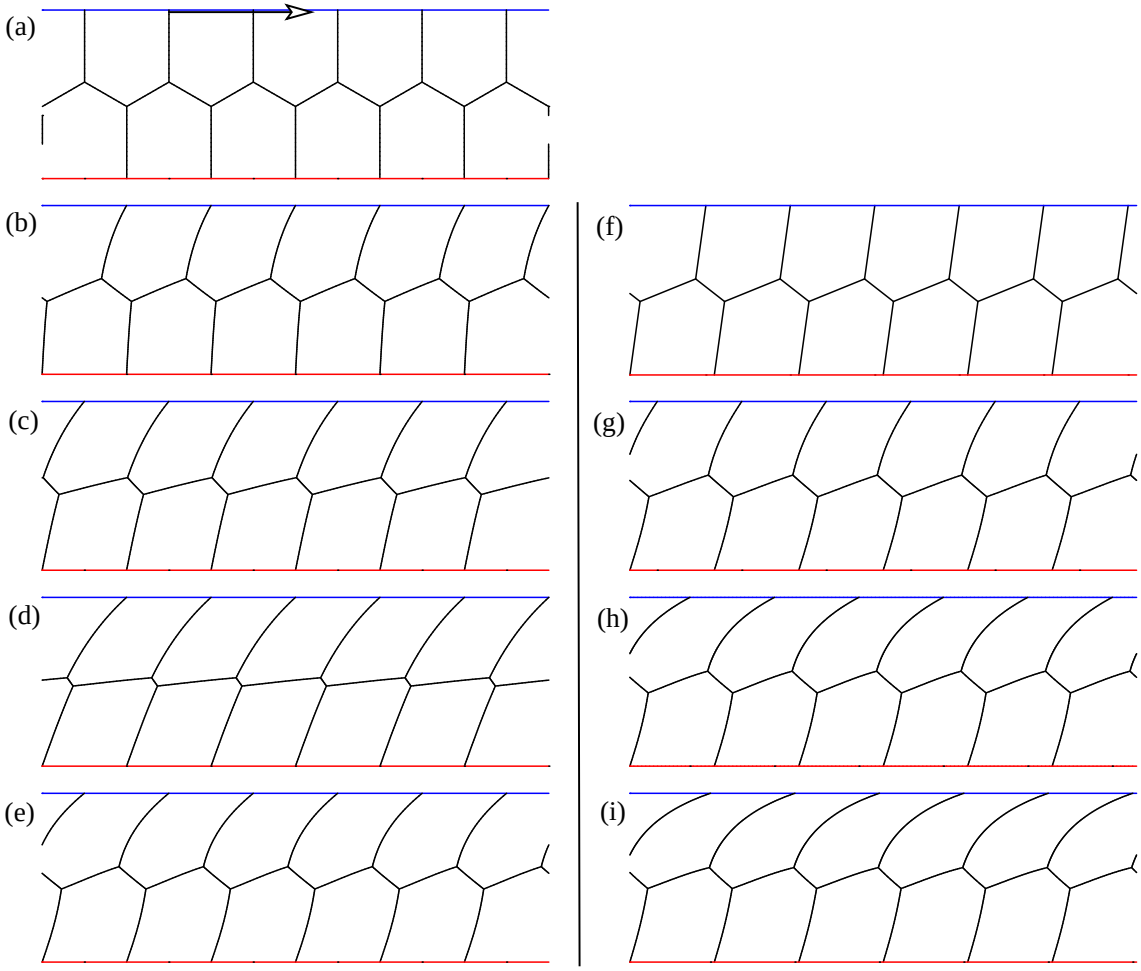

Fig. 6. Various stages in the shear of a staircase structure whose outer vertices are fixed on plane parallel walls. Recall that the viscous drag is *not* on the walls shown, but in the plane of the page. (a) The initial staircase structure, and the sense of the strain. The channel is of width $w = 2$ and the bubbles all have unit area. For strain-rate $\dot{\zeta} = 0.250$ (b)–(e) show the structure after equal increments in strain, with the six T1 events occurring between (d) and (e). The last four images show the structure not long after the T1 has occurred, as for (e), with strain-rates (f) $\dot{\zeta} = 0$ (quasi-static), (g) $\dot{\zeta} = 0.125$, (h) $\dot{\zeta} = 0.375$ and (i) $\dot{\zeta} = 0.500$.

films become increasingly deformed and thus the energy increases for given strain. At a critical value of strain six pairs of vertices meet and the resulting six T1 changes cause the line-length to drop rapidly. The motion then returns to a similar cycle as before, although note that motion is not precisely periodic; this is particularly evident for high strain-rate.

3.4 Coarsening-induced relaxation after a step-strain

We next investigate the competition between the two time-scales representing relaxation, T_λ, and coarsening, T_κ. To do this, we simulate the relaxation after an initial step strain of a two-dimensional sample of foam, while coarsening proceeds. This is the direct extension of the quasi-static simulation of Kermode (see [2], Fig. 8.13) to the viscous froth case.

We create a relaxed, periodic, polydisperse sample of $N = 100$ bubbles (a uniform distribution of areas between $A = 0$ and 2, with $\langle A \rangle = 1$) and perform an instantaneous unit step strain, as shown in figure 8. The strain is then held at a value of one. We allow gas-diffusion in the foam

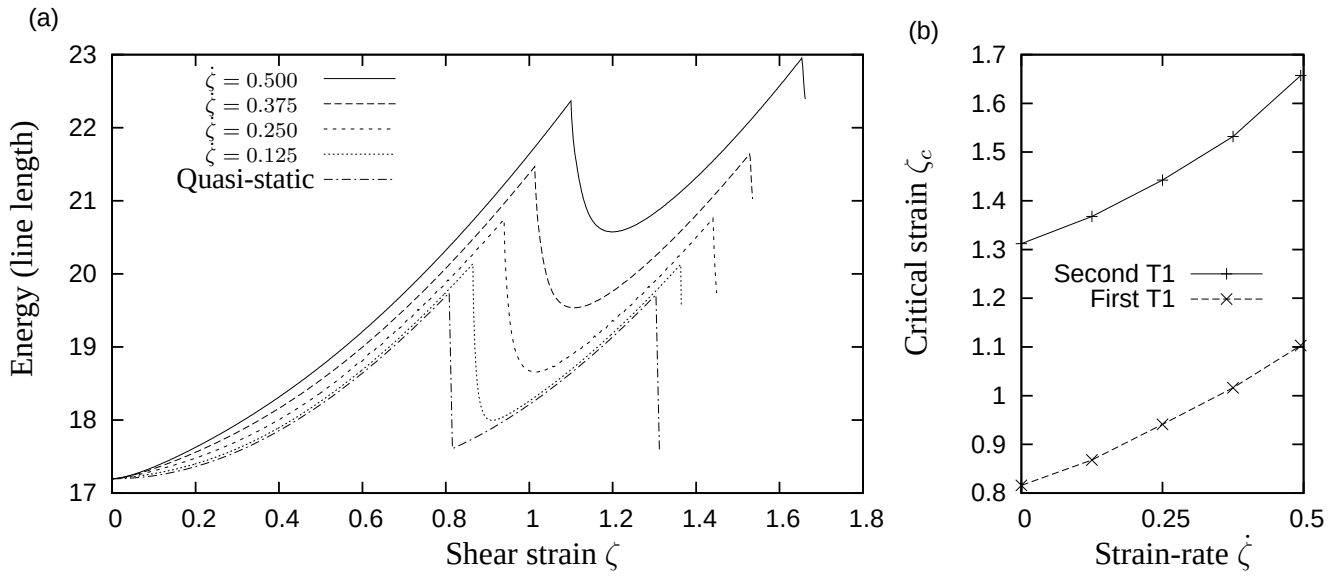

Fig. 7. (a) The energy (divided by surface tension γ) of the deformed staircase structures for a range of strain-rates $\dot{\zeta}$. The strain is $\zeta = d/w$, where d is the displacement of the moving wall. From these graphs it is clear where the T1s occur, so that in (b) we plot the critical strain ζ_c at which the T1s occur for given strain-rate. ζ_c increases (less than quadratically; exponent ≈ 1.45) with strain-rate.

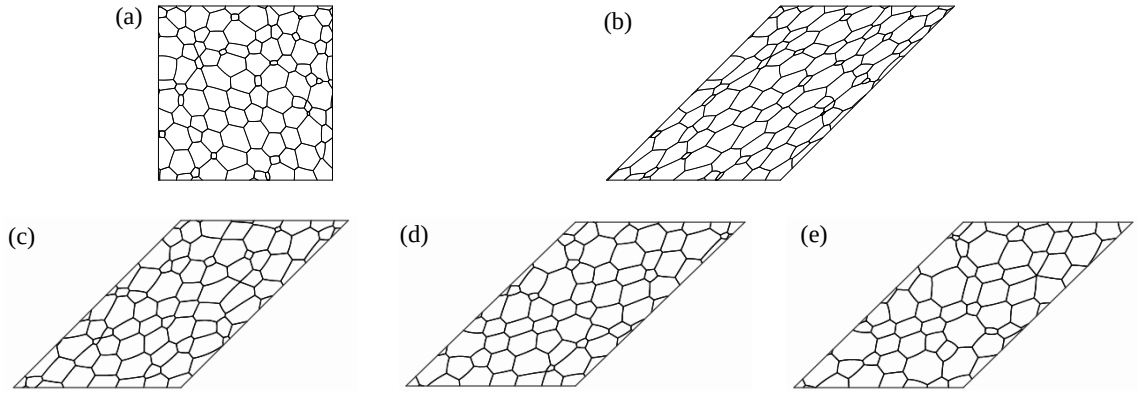

Fig. 8. Various stages in the evolution of foam coarsening after a unit step strain. (a) The initial relaxed foam of 100 bubbles with an average area of one. (b) The foam immediately after the strain is applied. (c) The foam at $t = 0.08$, (d) at $t = 0.16$ and (e) at $t = 0.24$.

to simulate coarsening as the viscous relaxation takes place. The area of a bubble with n sides is changed according to von Neumann's law:

$$\frac{\mathrm{dA}}{\mathrm{dt}} = \frac{1}{3}\pi\kappa(n-6). \tag{7}$$

We measure the stress in the foam by summing the orientations θ_i of each of the small edges

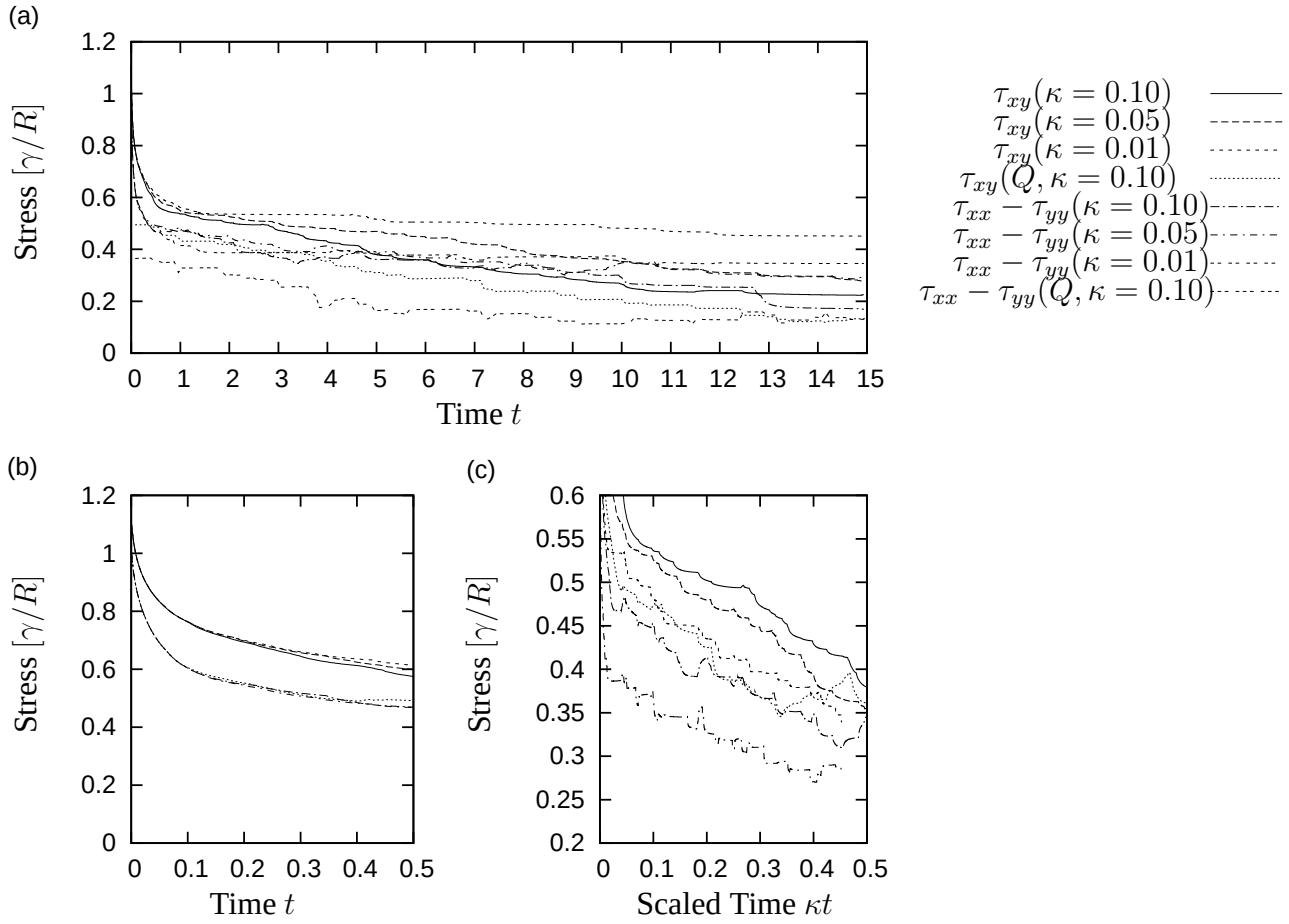

Fig. 9. The evolution of the shear stress and normal stress difference in a simulation in which the coarsening proceeds after an initial step strain of one. For illustrative purposes, three different diffusion constants κ are used in the viscous froth simulations, as indicated in the legend, and in one case the results are compared with the equivalent quasi-static simulation (marked Q). R is a measure of the average bubble area. (a) In the quasi-static case, the stresses are consistently below those with viscosity, because of the full and immediate relaxation. (b) With the viscous froth, all stresses show a rapid initial relaxation after the step strain. (c) Once the foam has relaxed from the strain, there is a slower decrease in stress driven by coarsening. Scaling the time with the diffusion constant shows that the essential behaviour in this regime is independent of coarsening rate, since all curves show a roughly linear decrease with the same slope.

i of length l_i that describe the films, resolved in x and y directions. The shear stress $\tau_{xy} = (2/NA)\sum_i \sin\theta_i \cos\theta_i$ and the normal stress difference $\tau_{xx} - \tau_{yy} = (2/NA)\sum_i \cos^2\theta_i - \sin^2\theta_i$ are shown in figure 9(a). We also show the results of a quasi-static simulation on a similar foam: in this case the stresses stay below those obtained from the viscous froth simulations, since there is complete relaxation at each step. With a coarsening rate of $\kappa = 0.1$, approximately 50 bubbles remain at time $t = 15$.

For each of the three diffusion constants chosen we see a rapid decrease of both normal stress difference and shear-stress, magnified in figure 9(b), followed by the more gradual "creep" due to coarsening [24]. In figure 9(c) we reduce the time axis so that all stresses are seen to decrease at the same rate. The most noticeable effects of including viscous drag are that (i) the initial decreases in energy and stress are resolved, and (ii) the data is smoothed out, and the sudden jumps (and ambiguity) evident in the results of quasi-static simulations are removed.

In future work we shall extend such work to simulate a range of rheological experiments that will elucidate the dynamics of coarsening foams. Examples include the increase of stress with start-up

strain and constant stress experiments. In these cases, all three time-scales play a role.

4 Summary

The viscous froth model, as described here, is straightforward to implement within the Surface Evolver. It provides a method for determining the response of dry 2D foams to perturbations that are rate-dependent and/or fast compared to the relaxation of the soap films to equilibrium. In addition, it retains the full geometrical details of the foam structure (bubble pressures and film curvatures), as for the quasi-static model but in contrast to most models of 2D *viscous* foam rheology. Now that its implementation is complete, at least in this basic mode of operation, there is a huge range of further experiments that will benefit from its predictive capabilities. At the same time, there *are* further effects to be added, as discussed above, and in due course their influence will be determined.

Acknowledgements

This work benefited from discussions with many people, not the least of whom were D. Weaire and K. Brakke, to whose Surface Evolver software I am now inextricably intertwined. I am grateful to N. Kern and S. Hutzler for passing on their knowledge of the viscous froth model, and to W. Drenckhan for exhausting discussions on its applicability. I. Cantat, M. Dennin, J. Glazier, F. Graner, R. Höhler and A. Kraynik all gave (mostly) constructive criticisms, and S. Cohen-Addad forced me to explain the model coherently (although any remaining errors are mine alone).

I am grateful for partial support from both the Ulysses France-Ireland Exchange Scheme and the European Space Agency, Contract 14308/00/NL/SH (AO-99-031) CCN 002 MAP Project AO-99-075.

References

[1] N. Kern, D. Weaire, A. Martin, S. Hutzler and S.J. Cox. 2004 The two-dimensional viscous froth model for foam dynamics. *Phys. Rev. E* **70**:041411.
[2] D. Weaire and S. Hutzler. 1999 *The Physics of Foams*. Clarendon Press, Oxford.
[3] K. Brakke. 1992 The Surface Evolver. *Exp. Math.* **1**:141–165.
[4] T. Okuzono, K. Kawasaki and T. Nagai. 1993 Rheology of Random Foams. *J. Rheol.* **37**: 571–586.
[5] T. Okuzono and K. Kawasaki. 1995 Intermittent flow behavior of random foams: A computer experiment on foam rheology. *Phys. Rev. E* **51**:1246–1253.
[6] I. Cantat and R. Delannay. 2003 Dynamical transition induced by large bubbles in two-dimensional foam flows. *Phys. Rev. E* **67**:031501.
[7] R.L. Fullman 1952 *Boundary Migration During Grain Growth* pp. 179–207. American Society for Metals, Cleveland.
[8] D.J. Durian. 1995 Foam Mechanics at the Bubble Scale. *Phys. Rev. Lett.* **75**:4780–4783.
[9] D. Weaire and F. Bolton. 1990 Rigidity Loss Transition in a Disordered 2D Froth. *Phys. Rev. Lett.* **65**:3449.

[10] Y. Jiang, P.J. Swart, A. Saxena, M. Asipauskas and J.A. Glazier. 1999 Hysteresis and Avalanches in two-dimensional foam rheology simulations. *Phys. Rev. E* **59**:5819–5832.
[11] Q. Sun and S. Hutzler. 2004 Lattice gas simulations of two-dimensional liquid foams. *Rheol. Acta* **43**:567-574.
[12] I. Cantat, N. Kern and R. Delannay. 2004 Dissipation in foam flowing through narrow channels. *Europhys. Letts.* **65**:726–732.
[13] D.A. Reinelt and A.M. Kraynik. 1989 Viscous Effects in the Rheology of Foams and Concentrated Emulsions. *J. Colloid Interf. Sci* **132**:491–503.
[14] R. Delanney, I. Cantat and J. Etrillard. 2004. Viscous force exerted by a wall on a foam. Presentation at EuFoam.
[15] F.P. Bretherton. 1961 The motion of long bubbles in tubes. *J. Fluid Mech.* **10**:166–188.
[16] W. Drenckhan. 2004 *Stability and motion of foams and films in confined geometries*. PhD thesis. Department of Physics, Trinity College, University of Dublin.
[17] G. Delaney, S. Cox and W. Drenckhan. 2004. The two-dimensional viscous froth model for foam dynamics. Poster at EuFoam.
[18] W. Drenckhan, S. Cox, D. Weaire and S. Hutzler. 2004. Foam rheology with ordered foam structures. Presentation at EuFoam.
[19] D. Weaire and N. Rivier. 1984 Soap, cells and statistics–random patterns in two dimensions. *Contemp. Phys.* **25**:59–99.
[20] G. Debregeas, H. Tabuteau and J.M. di Meglio. 2001 Deformation and flow of a two-dimensional foam under continuous shear. *Phys. Rev. Lett.* **87**:178305.
[21] J. Lauridsen, M. Twardos and M. Dennin. 2002 Shear-induced stress relaxation in a two-dimensional wet foam. *Phys. Rev. Lett.* **89**:098303.
[22] E. Janiaud and F. Graner. 2004 Foam in a two-dimensional Couette shear: a local measurement of bubble deformation. *J. Fluid Mech.* **In press**.
[23] S.J. Cox, D. Weaire and J.A. Glazier. 2004 The rheology of two-dimensional foams. *Rheol. Acta* **43**:442–448.
[24] S. Cohen-Addad, R. Höhler and Y. Khidas. 2004 Origin of the Slow Viscoelastic Response of Aqueous Foams. *Phys. Rev. Lett.* **93**:028302.
[25] K. Brakke. 2004. Private Communication.

A Appendix: Implementation of the Viscous Froth Model in the Surface Evolver

In order to implement the viscous froth model in the Surface Evolver, we write an Evolver datafile in the usual way, including any necessary volume and boundary constraints. We first **refine** (Evolver keywords are given hereafter in bold) and iterate to convergence to create a discretized network of films at equilibrium. We will use the notation that many short *edges* make up a film, and that two edges meet at a *point*, while three edges or films meet at a *vertex*, in contrast to the usual Surface Evolver notation. At all times the length l of each edge is kept within a certain range, $l_{min} <= l <= l_{max}$, where l_{min} represents the length of a film at which a T1 process may occur. We retain a small value for l_{min} here (usually $l_{min} = 0.01$ for bubbles of area close to one).

We then replace the normal **g** iteration command with (2) as follows. Firstly, all bubble pressures are set to zero and all volume constraints turned off. The curvature K at each point is then found by performing a length-minimizing **g** iteration without allowing motion (i.e. with **scale** zero). We then set the **scale** to be equal to a time-step δt.

The pressure p_i of each bubble, in the case where the exponent α in (2) is equal to one, is found by integrating this equation of motion around the boundary of each bubble, to show that

$$\frac{\mathrm{dA_i}}{\mathrm{dt}} = \frac{\pi}{3}\left(n_i - 6\right) + \sum_{j \neq i}\left(p_i - p_j\right) l_{ij}, \tag{A.1}$$

for a bubble i having n_i sides. The quantity l_{ij} is the length of the film separating bubble i from j and is zero for all bubbles j that do not touch i. Given the change in volume at each step (for example from von Neumann's law (7), or as a correction to any numerical drift in volume) and the number of sides and perimeter of each bubble, we now have a matrix equation for the pressures p_i. We solve this using the the Evolver's **matrix_inverse** command and return it as an **attribute** to each **facet** (bubble), so that the necessary pressure differences Δp can be calculated.

Brakke [25] has suggested an alternative method of calculation, in which the pressures are found as an additional energy **quantity** which performs the integration of edge length around each bubble. The bubble area constraints are enforced with **area normalization** mode. At the time of writing, this method offers only a small saving in time, at the expense of difficulty in defining the additional quantities for bubbles lying on boundaries and constraints (e.g. walls). We therefore use it only for unconstrained foams.

The motion of each point at position $\underline{x}$ in the current time-step can then be calculated from (2):

$$\underline{x}_{new} = \underline{x}_{old} + \underline{n}\,\delta t\left(\Delta P - \gamma K\right)/\lambda \tag{A.2}$$

where $\underline{n}$ is the normal to each point, given by the respective indices of **vertex_normal**.

For bubbles of average area unity and edge-length bounds as given above, we find that a time-step of $\delta t \approx 1 \times 10^{-4}$ is appropriate. As the average bubble area is varied, the edge-length bounds and time-step may be changed appropriately.